Theoretical analyses of multiple quasi-phase-matched third-harmonic generation for all configurations

Ding Zhu, Chao Zhang, Yi-qiang Qin,* and Yong-yuan Zhu

National Laboratory of Solid State Microstructures, College of Engineering and Applied Sciences, Nanjing University, Nanjing 210093, China

(Received 10 March 2012; revised manuscript received 20 June 2012; published 6 August 2012)

A general theory for multiple quasi-phase-matched third-harmonic generation is investigated systematically. We find that there are up to 24 configurations for third-harmonic generation by cascaded two-parametric processes. All these configurations can be divided into three categories based on the coupling types of the harmonic fields. Each category has a set of coupled wave equations that describe its characteristics. The analytical solutions reveal some features, such as the polarization tuning and quasi-phase-matched gap effect.

DOI: 10.1103/PhysRevE.86.026602 PACS number(s): 46.90.+s, 42.65.−k

I. INTRODUCTION

The first experimental observation that came to be known as quasicrystals was made by Shechtman *et al*. in 1982 and reported in print two years later [1]. Since then, the fields of quasicrystals and quasiperiodic structures has attracted a lot of attention. Besides the studies focused on their structural and physical properties [2,3], much effort has been devoted to the applications of quasicrystals and quasiperiodic structures in optics and photonics. For example, the quasiperiodic envelope solitons have been realized [4], and the photonic band-gap effect in two-dimensional Penrose tiled photonic quasicrystals have been studied [5,6]. In particular, the quasiperiodic optical superlattice can be used for efficient third-harmonic generation (THG) [7], where multiple quasi-phase-matched (MQPM) nonlinear processes of second-harmonic generation (SHG) and sum-frequency generation (SFG) are realized simultaneously by two incommensurate reciprocal vectors, indicating that the quasiperiodic structures may be the best candidates for MQPM nonlinear optical interactions.

It is well known that THG is widely used for the extension of a laser source to short wavelengths. But due to the extremely low third-order nonlinearity, the direct THG resulting from a third-order nonlinear process is of little practical importance. The first efficient THG was achieved by MQPM nonlinear interactions with cascaded second-order nonlinearities. To date, most experimental and theoretical studies of MQPM THG in nonlinear crystals have concentrated on the largest second-order nonlinear coefficient d_{33} (corresponding to cascaded two $ee \rightarrow e$ processes) for its highest nonlinear coupling strength [8–11]. However, other nonlinear coefficients such as d_{32} and d_{24} can also be used in some cases [12–15], where non-$ee \rightarrow e$ processes such as $oo \rightarrow e$ and $oe \rightarrow o$ can be efficiently achieved. Here "e" denotes the extraordinary wave and "o" the ordinary wave.

Recently, the polarization tuning of cascaded interactions with one $ee \rightarrow e$ process and one non-$ee \rightarrow e$ process in lithium niobate (LN) nonlinear photonic crystals has been observed [16], but not well studied in theory. The MQPM THG by two non-$ee \rightarrow e$-type processes has not been studied until now. In this article, we try to not only investigate the MQPM THG with two non-$ee \rightarrow e$ processes, but also construct a general theory of THG for all types of configurations with the two cascaded $ee \rightarrow e$ processes being a special case.

II. THEORETICAL RESULTS AND DISCUSSION

The scheme of cascaded THG could be described as

$$\omega_1 + \omega_1 \leftrightarrow \omega_2, \tag{1}$$

$$\omega_1 + \omega_2 \leftrightarrow \omega_3. \tag{2}$$

The subscripts 1, 2, 3 (which could be either the ordinary or extraordinary wave) refer respectively to the fundamental, second harmonic (SH), and third harmonic (TH). The fundamental is divided into a horizontally polarized component and a vertically polarized component with respect to the orientation of the crystal axis.

It can be easily seen that Eq. (1) has six combinations: three possibilities on the left (ee, oo, eo, or oe) and two possibilities on the right (e or o). Equation (2) has four combinations (the polarization of ω_2 has been fixed by the first process, so there are two possibilities remaining on the left and two possibilities on the right). Therefore there are a total of 24 possible configurations. For each case, we could deduce a set of coupled wave equations to describe its coupling characteristics. Surely these discussions would be quite complicated. Can we simplify these 24 configurations and describe them with just a few equations? Fortunately, the answer is positive.

Actually, in the coupled wave equations o and e are commutative. For example, the following two configurations, $e_1o_1 \rightarrow o_2$, $e_1o_2 \rightarrow e_3$ and $e_1o_1 \rightarrow e_2$, $o_1e_2 \rightarrow e_3$, both use two polarized components of the fundamental to generate SH, followed by SH and one polarized component of the fundamental to generate TH. A careful analysis shows that whether SH (or TH) is horizontally or vertically polarized makes no difference. The two configurations have common energy conversion characteristics. In this way, all 24 cases could be simplified into only three categories. Each of them is described by a unified set of coupled wave equations. Table I lists all the cases. The second column in Table I illustrates the schematic interactions of each category. The red (circle) and pink (light gray), green (gray), and blue (gray) balls represent the fundamental, SH, and TH photons, respectively. The two orthogonally polarized fundamental photons are commutative, while the SH or TH

*Corresponding author: yqqin@nju.edu.cn

TABLE I. Classification of MQPM THG.

	Fundamental Second harmonic Third harmonic	Related processes
Category I	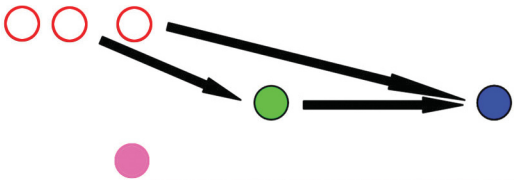	$e_1e_1 \to e_2,\ e_1e_2 \to e_3;\ e_1e_1 \to e_2,\ e_1e_2 \to o_3;$ $e_1e_1 \to o_2,\ e_1o_2 \to e_3;\ e_1e_1 \to o_2,\ e_1o_2 \to o_3;$ $o_1o_1 \to e_2,\ o_1e_2 \to e_3;\ o_1o_1 \to e_2,\ o_1e_2 \to o_3;$ $o_1o_1 \to o_2,\ o_1o_2 \to e_3;\ o_1o_1 \to o_2,\ o_1o_2 \to o_3$
Category II	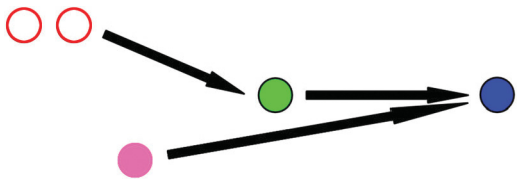	$e_1e_1 \to e_2,\ o_1e_2 \to e_3;\ e_1e_1 \to e_2,\ o_1e_2 \to o_3;$ $e_1e_1 \to o_2,\ o_1o_2 \to e_3;\ e_1e_1 \to o_2,\ o_1o_2 \to o_3;$ $o_1o_1 \to e_2,\ e_1e_2 \to e_3;\ o_1o_1 \to e_2,\ e_1e_2 \to o_3;$ $o_1o_1 \to o_2,\ e_1o_2 \to e_3;\ o_1o_1 \to o_2,\ e_1o_2 \to o_3$
Category III	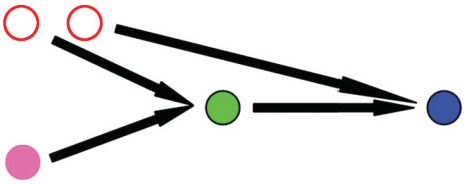	$e_1o_1 \to e_2,\ e_1e_2 \to e_3;\ e_1o_1 \to e_2,\ e_1e_2 \to o_3;$ $e_1o_1 \to o_2,\ e_1o_2 \to e_3;\ e_1o_1 \to o_2,\ e_1o_2 \to o_3;$ $e_1o_1 \to e_2,\ o_1e_2 \to e_3;\ e_1o_1 \to e_2,\ o_1e_2 \to o_3;$ $e_1o_1 \to o_2,\ o_1o_2 \to e_3;\ e_1o_1 \to o_2,\ o_1o_2 \to o_3$

photons could be any one of the two orthogonally polarized states. The specific configurations included in each category are all shown in the third column. Given in Table II are the coupled wave equations for these three categories, which are responsible for their totally different behavior.

In Table II, κ_1 and κ_2 are the nonlinear coupling coefficients. A_{ij} is the defined new field variable; the asterisk denotes its complex conjugation:

$$A_{ij} = \sqrt{\frac{n_{ij}}{\omega_i}} E_{ij} \quad (i = 1,2,3; \quad j = a,b,c,d). \tag{3}$$

E_{ij}, ω_i, and n_{ij} are the electric field, the angular frequency, and the refractive index, respectively. The subscripts 1,2,3 refer respectively to fundamental, SH, and TH with $j = a,b,c,d$ denoting their polarizations. It is noted that c and d could take e or o arbitrarily, but the choices of a and b are interdependent, i.e. when a is o, b will be e; when a is e, b will be o; $k_a^{\omega}(k_b^{\omega})$, $k_c^{2\omega}$ and $k_d^{3\omega}$ are the wave vectors of fundamental, SH, and TH, respectively; Δk_1 and Δk_2 are the wave-vector mismatches; G_1, G_2 and f_1, f_2 are the reciprocal vectors and the associated Fourier coefficients of the domain engineered structure; d_1 and d_2 are the nonlinear optical coefficients depending on the nonlinear crystal and the configuration in Table I. c is the speed of light in vacuum. Below we take LN as an example to investigate their detailed physical properties.

Category I: SH is generated by one polarized component of the fundamental, and TH is generated by mixing of SH and the same component of the fundamental. This category

TABLE II. The coupled wave equations for three categories.

	Unified coupled wave equations	Corresponding coefficients
Category I	$\begin{cases} \frac{dA_{1a}}{dx} = -i\kappa_1 A_{1a}^* A_{2c} \exp(-i\Delta k_1 x) - i\kappa_2 A_{2c}^* A_{3d} \exp(-i\Delta k_2 x) \\ \frac{dA_{2c}}{dx} = -i\frac{\kappa_1}{2} A_{1a}^2 \exp(i\Delta k_1 x) - i\kappa_2 A_{1a}^* A_{3d} \exp(-i\Delta k_2 x) \\ \frac{dA_{3d}}{dx} = -i\kappa_2 A_{1a} A_{2c} \exp(i\Delta k_2 x) \end{cases}$	$\kappa_1 = \frac{f_1 d_1}{c}\sqrt{\frac{\omega_1\omega_1\omega_2}{n_{1a}n_{1a}n_{2c}}}, \quad \kappa_2 = \frac{f_2 d_2}{c}\sqrt{\frac{\omega_1\omega_2\omega_3}{n_{1a}n_{2c}n_{3d}}}$ $\Delta k_1 = k_c^{2\omega} - k_a^{\omega} - k_a^{\omega} - G_1$ $\Delta k_2 = k_d^{3\omega} - k_c^{2\omega} - k_a^{\omega} - G_2$
Category II	$\begin{cases} \frac{dA_{1a}}{dx} = -i\kappa_1 A_{1a}^* A_{2c} \exp(-i\Delta k_1 x) \\ \frac{dA_{1b}}{dx} = -i\kappa_2 A_{2c}^* A_{3d} \exp(-i\Delta k_2 x) \\ \frac{dA_{2c}}{dx} = -i\frac{\kappa_1}{2} A_{1a}^2 \exp(i\Delta k_1 x) - i\kappa_2 A_{1b}^* A_{3d} \exp(-i\Delta k_2 x) \\ \frac{dA_{3d}}{dx} = -i\kappa_2 A_{1b} A_{2c} \exp(i\Delta k_2 x) \end{cases}$	$\kappa_1 = \frac{f_1 d_1}{c}\sqrt{\frac{\omega_1\omega_1\omega_2}{n_{1a}n_{1a}n_{2c}}}, \quad \kappa_2 = \frac{f_2 d_2}{c}\sqrt{\frac{\omega_1\omega_2\omega_3}{n_{1b}n_{2c}n_{3d}}}$ $\Delta k_1 = k_c^{2\omega} - k_a^{\omega} - k_a^{\omega} - G_1$ $\Delta k_2 = k_d^{3\omega} - k_c^{2\omega} - k_b^{\omega} - G_2$
Category III	$\begin{cases} \frac{dA_{1a}}{dx} = -i\kappa_1 A_{1b}^* A_{2c} \exp(-i\Delta k_1 x) - i\kappa_2 A_{2c}^* A_{3d} \exp(-i\Delta k_2 x) \\ \frac{dA_{1b}}{dx} = -i\kappa_1 A_{1a}^* A_{2c} \exp(-i\Delta k_1 x) \\ \frac{dA_{2c}}{dx} = -i\kappa_1 A_{1a} A_{1b} \exp(i\Delta k_1 x) - i\kappa_2 A_{1a}^* A_{3d} \exp(-i\Delta k_2 x) \\ \frac{dA_{3d}}{dx} = -i\kappa_2 A_{1a} A_{2c} \exp(i\Delta k_2 x) \end{cases}$	$\kappa_1 = \frac{f_1 d_1}{c}\sqrt{\frac{\omega_1\omega_1\omega_2}{n_{1a}n_{1b}n_{2c}}}, \quad \kappa_2 = \frac{f_2 d_2}{c}\sqrt{\frac{\omega_1\omega_2\omega_3}{n_{1a}n_{2c}n_{3d}}}$ $\Delta k_1 = k_c^{2\omega} - k_b^{\omega} - k_a^{\omega} - G_1$ $\Delta k_2 = k_d^{3\omega} - k_c^{2\omega} - k_a^{\omega} - G_2$

has eight configurations, each of which contains the $e_1e_1 \rightarrow e_2$, $e_1e_2 \rightarrow e_3$ MQPM THG. This configuration has been theoretically studied by Zhang *et al.* [17]. In that work, the authors deduced an analytical solution about the relationship of the maximum TH conversion efficiency (represented by $\eta_{3\,\max}$) with the ratio of SHG coupling coefficient and SFG coupling coefficient (represented by t). A crucial value $t/2 = \cos(\{[1-(t/2)^2]^{1/2}/t\}\ln 3)$ (where $t \approx 0.8858$) was obtained, with which the energy of the fundamental could be transferred to TH completely. When $t < 0.8858$, $\eta_{3\,\max}$ cannot be written in an analytical form but can be numerically calculated. When $t \geqslant 0.8858$, $\eta_{3\,\max}$ was deduced to be

$$\eta_{3\,\max}(t) = \begin{cases} 3\exp\left\{-\frac{t}{\left[1-\left(\frac{t}{2}\right)^2\right]^{1/2}}\arccos\left(t/2\right)\right\} & 0.8858 \leqslant t < 2 \\ 3\exp(-2) & t = 2 \\ 3\left\{\frac{t}{2}+\left[\left(\frac{t}{2}\right)^2-1\right]^{1/2}\right\}^{-\frac{t}{[(t/2)^2-1]^{1/2}}} & t > 2 \end{cases}. \tag{4}$$

With $t \rightarrow 0$ and $t \rightarrow \infty$, $\eta_{3\,\max}(t)$ will reduce to zero. Although the authors studied only one case, the results are valid for all the configurations belonging to category I (see Table I). It is worth noting that this category uses only one polarized component of the fundamental and $\eta_{3\,\max}$ is only related to the ratio of the two coupling coefficients t.

Category II: SH is generated by one polarized component of the fundamental, and TH is generated by mixing of SH and another orthogonal component of the fundamental. This category also contains eight configurations (see Table I). We take the $o_1o_1 \rightarrow e_2$, $e_1e_2 \rightarrow e_3$ configuration of category II as an example. Hence subscripts a, b, c, d are set as o, e, e, e, respectively; d_1 and d_2 are equal to d_{32} and d_{33}, respectively. Under MQPM conditions ($\Delta k_1 = \Delta k_2 = 0$), the involved harmonics are coupled strongly. Let $y_{1o} = A_{1o}$, $y_{1e} = A_{1e}$, $y_{2e} = -iA_{2e}$ and $y_{3e} = A_{3e}$, The coupled wave equations could be simplified into real equations:

$$\begin{cases} y'_{1o} = \kappa_1 y_{1o} y_{2e} \\ y'_{1e} = -\kappa_2 y_{2e} y_{3e} \\ y'_{2e} = -\frac{\kappa_1}{2} y_{1o}^2 - \kappa_2 y_{1e} y_{3e} \\ y'_{3e} = \kappa_2 y_{1e} y_{2e} \end{cases}. \tag{5}$$

Three integrals of motion exist in this system:

$$y_{1o}^2 + y_{1e}^2 + 2y_{2e}^2 + 3y_{3e}^2 = y_{1o}^2(0) + y_{1e}^2(0), \tag{6}$$

$$y_{1e}^2 + y_{3e}^2 = y_{1e}^2(0), \tag{7}$$

$$\kappa_2 \ln \frac{y_{1o}^2}{y_{1o}^2(0)} = 2\kappa_1 \arcsin \frac{y_{3e}}{y_{1e}(0)}. \tag{8}$$

The first one corresponds to the energy conservation. Suppose that $y_{3e\,\max}$ is the maximum value of y_{3e} at $y'_{3e} = 0$; the three integrals of motion lead to an analytical solution of maximum TH conversion efficiency $\eta_{3\,\max} = 3y_{3e\,\max}^2/[y_{1o}^2(0) + y_{1e}^2(0)]$ with normalized boundary conditions as follows:

For $y_{1e} = 0$,

$$\eta_{3\,\max} = 3\cos^2\theta. \tag{9}$$

For $y_{2e} = 0$,

$$\eta_{3\,\max} = \frac{3}{2}\cos^2\theta\left\{1-\cos\left[\frac{1}{t}\ln\left(1-\frac{2\eta_{3\,\max}}{3\sin^2\theta}\right)\right]\right\}. \tag{10}$$

While $t = \kappa_1/\kappa_2$ is the ratio of two coupling coefficients, it is mainly determined by the domain engineered structure. $\theta = \arctan[y_{1o}(0)/y_{1e}(0)]$ is the angle between the polarization direction of the fundamental and the z axis of the crystal, which represents the fundamental energy distribution in two orthogonal directions. The two solutions are separated approximately by a continuous boundary:

$$\tan\theta_B = \sqrt{\frac{2}{1-e^{-\pi t}}}. \tag{11}$$

Here θ_B is the function of t. Region $\{0 \leqslant t \leqslant \infty,\ \theta_B(t) < \theta \leqslant 90^\circ\}$ is valid for Eq. (9) and region $\{0 \leqslant t \leqslant \infty,\ 0^\circ \leqslant \theta \leqslant \theta_B(t)\}$ is valid for Eq. (10). It is interesting to note that for Eq. (9), $\eta_{3\,\max}$ has no relation to t, which means for certain $\theta > \theta_B$, the maximum conversion efficiency of TH is a constant. Basically, this characteristic suggests that the ratio of two coupling coefficients is not the limiting factor of the efficiency and $\eta_{3\,\max}$ depends only on the energy distribution of the fundamental. Such a property is favorable for practical applications, which could provide more flexibility for the design of QPM domain structure and reduce the influence of any domain structure divergence resulting from the fabrication. Equation (10) is an implicit function and $\eta_{3\,\max}$ cannot be explicitly solved, but rather must be numerically solved. Figure 1 shows the visualization of the two solutions, which construct the two faces of the $\eta_{3\,\max}$ graph.

When $\theta > \theta_B$, y_{1o} exceeds the demand, making TH conversion efficiency reach its maximum under the condition of $y_{1e} = 0$. When $\theta < \theta_B$, y_{1o} is less than the optimal value. According to Eq. (5), $y_{2e} = 0$ becomes the extremum condition for $\eta_{3\,\max}$. Only when $\theta = \theta_B$ is the SHG process balanced by the SFG process and $\eta_{3\,\max}$ reaches its optimal value. This situation corresponds to the ridge line of Fig. 1. The projection of $\eta_{3\,\max}$ graph on the $\eta_{3\,\max} - t$ coordinate plane is shown in Fig. 2, where the ridge line is given by

$$\eta_{3\,\max} = \frac{3(1-e^{-\pi t})}{3-e^{-\pi t}}. \tag{12}$$

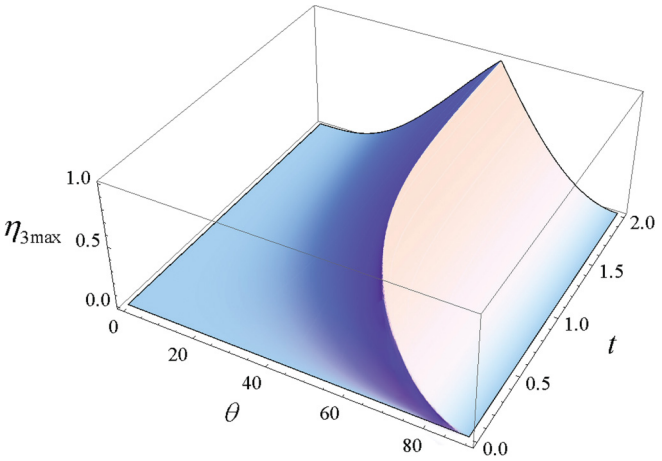

FIG. 1. (Color online) The visualization of maximum TH conversion efficiency $\eta_{3\max}$ on the ratio of SHG and SFG coupling coefficients t and the fundamental polarization angle θ for category II.

In category I, there exists a crucial value $t \approx 0.8858$, with which 100% TH conversion efficiency could be realized [17], while in category II, there is no such crucial value. $\eta_{3\max}$ monotonically increases with t; when $t \to \infty$, $\eta_{3\max} \to 100\%$. Although 100% TH conversion efficiency cannot be strictly met, it exceeds 90% when $t \geqslant 0.7$. As can be seen in Fig. 2, such a frequency conversion characteristic is favorable for efficient THG. Basically, it results from the fact of the polarization-dependent property in category II. The additional flexibility of polarization tuning enables the great adjustability of the harmonic conversion processes and leads to better THG performance.

To further illustrate the evolution processes of the involved harmonics inside the crystal, we select two cases of $\eta_{3\max}$ located on both sides of the ridge line. As shown in Fig. 3, these two cases have quite different harmonic evolution properties. In Fig. 3(a), the decline of y_{1o} makes the energy transfer to y_{2e} continuously, while y_{3e} reaches its maximum at $y_{1e} = 0$ and periodically oscillates between $y_{3\max}$ and zero. In Fig. 3(b), the

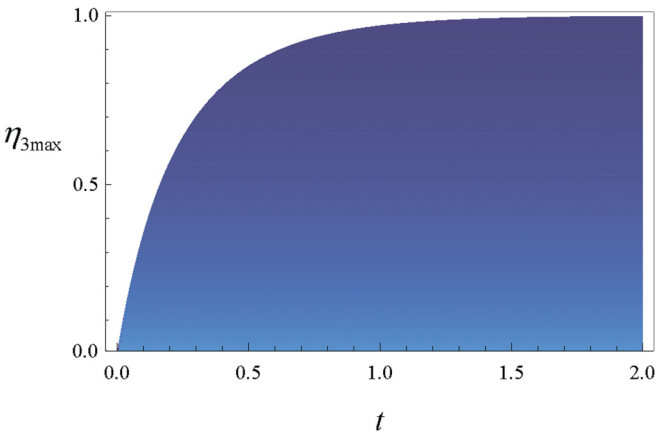

FIG. 2. (Color online) The projection of $\eta_{3\max}$ graph on the $\eta_{3\max} - t$ coordinate plane for category II. The edge of the graph represents $\eta_{3\max}$ at θ_B.

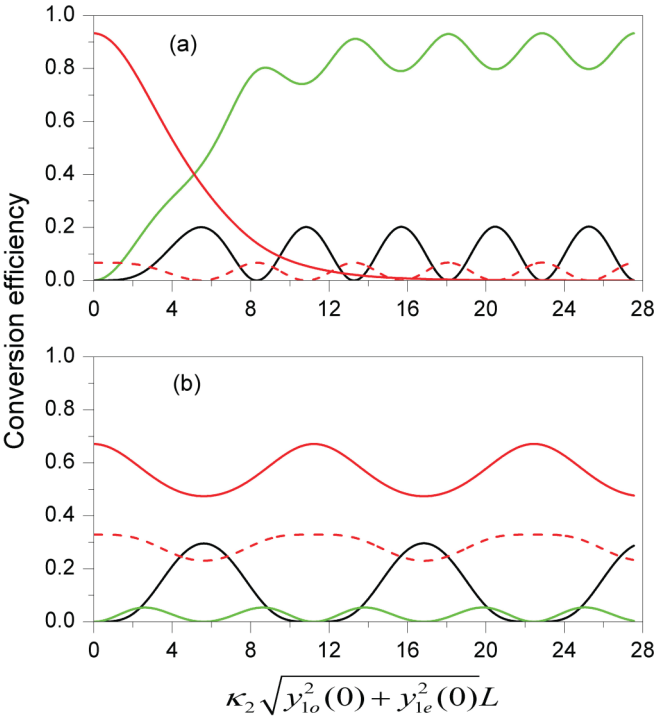

FIG. 3. (Color online) The dependence of harmonic intensities on the equivalent crystal length $\kappa_2\sqrt{y_{1o}^2(0)+y_{1e}^2(0)}L$ on both sides of the ridge line [represented by $\theta_B(0.3) = 61.1^\circ$]. (a) $t = 0.3$, $\theta = 75^\circ$; (b) $t = 0.3$, $\theta = 55^\circ$. The red (dark gray), dashed, green (light gray), and black lines represent y_{1o}, y_{1e}, y_{2e}, and y_{3e},respectively.

situation is quite different. y_{3e} goes to its maximum at $y_{2e} = 0$ and all the waves involved oscillate periodically. These two cases represent the typical features of the two regions located on both sides of the ridge line.

Category III: SH is generated by two orthogonally polarized components of the fundamental, and TH is generated by

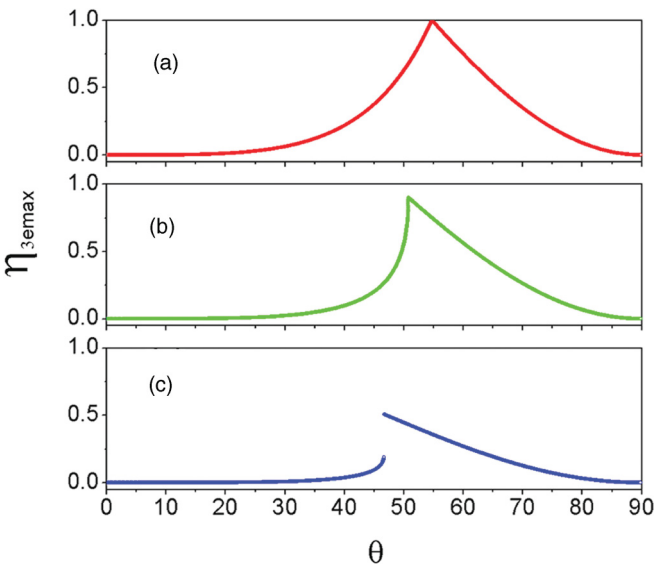

FIG. 4. (Color online) The dependences of $\eta_{3e\max}$ on the fundamental polarization angle θ for (a) $t = 1$, (b) $t = \sqrt{3}$, and (c) $t = 3$, respectively.

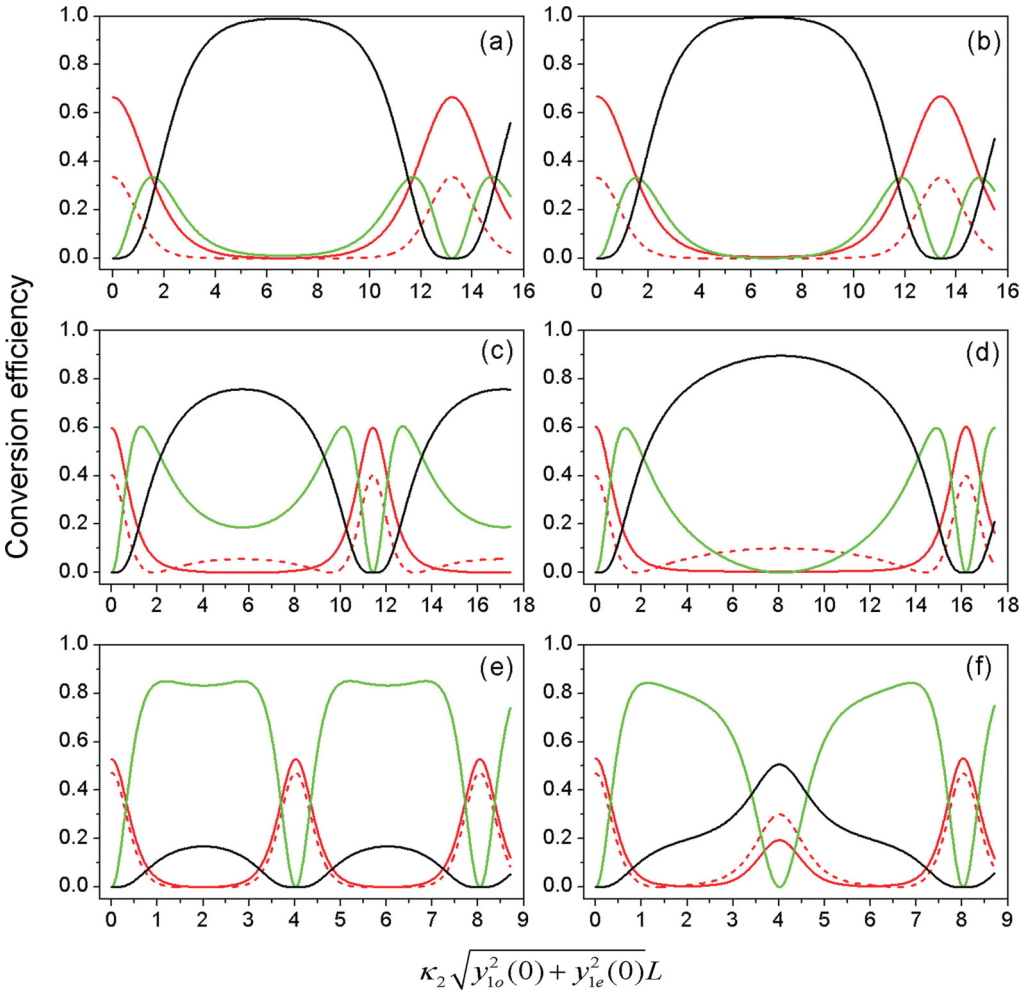

FIG. 5. (Color online) The dependence of the harmonic intensities on the equivalent crystal length on both sides of the ridge line for different t. (a) $t = 1$, $\theta = \theta_B(1) - 0.1°$; (b) $t = 1$, $\theta = \theta_B(1) + 0.1°$; (c) $t = \sqrt{3}$, $\theta = \theta_B(\sqrt{3}) - 0.1°$; (d) $t = \sqrt{3}$, $\theta = \theta_B(\sqrt{3}) + 0.1°$; (e) $t = 3$, $\theta = \theta_B(3) - 0.1°$; (f) $t = 3$, $\theta = \theta_B(3) + 0.1°$. The red (dark gray), dashed, green (light gray), and black lines represent y_{1o}, y_{1e}, y_{2o}, and y_{3e}, respectively.

mixing of SH and one polarized component of the fundamental. The cascaded $o_1e_1 \rightarrow o_2$, $o_1o_2 \rightarrow e_3$ THG processes belonging to category III were studied and the analytical solution of $\eta_{3e\,\max}$ was deduced in our previous work [18]. Similar to category I, category III also has a crucial value. When $t = 1$ and $\theta = \arctan\sqrt{2}$, $\eta_{3e\,\max}$ is 100%. In the meantime, the schemes of category III are polarization dependent, and like category II, the $\eta_{3e\,\max}$ graph is also constructed by two faces. When $t \leqslant \sqrt{3}$, the two faces are continuous on the ridge line. But when $t > \sqrt{3}$, the two faces split and a wide gap appears. This is the so called QPM gap effect, which only appears in category III.

Figure 4 shows the profiles of $\eta_{3e\,\max}$ graph for three typical points: $t = 1$, $\sqrt{3}$, and 3, which directly show the mentioned effect. Generally, $t = \kappa_1/\kappa_2$ represents the ratio of coupling strength between SHG and SFG processes. With t increasing from 1 to $\sqrt{3}$, the balance of energy transfer between SHG and SFG is gradually broken, leading to a significant decline of $\eta_{3e\,\max}$, whereas when $t > \sqrt{3}$, the balance is broken and $\eta_{3e\,\max}$ is discontinuous on the ridge line. When $t \leqslant \sqrt{3}$, one value of $\eta_{3e\,\max}$ corresponds to two polarization angles of the fundamental, while when $t > \sqrt{3}$, one value of $\eta_{3e\,\max}$ corresponds to one or two polarization angles of the fundamental.

To study the QPM gap effect in detail, we pick out six typical points from Fig. 4, which are located on both sides of the ridge line for $\pm 0.1°$ of the fundamental critical angle $\theta_B(t)$. The evolution processes of the involved harmonics inside the crystal are viewed for each point. Figure 5 shows the dependence of normalized harmonic intensities on the equivalent length $\kappa_2\sqrt{y_{1o}^2(0) + y_{1e}^2(0)}L$. Figures 5(a) and 5(b) correspond to the situation at $t = 1$. The maximum and the oscillation period of THG are continuous on the boundary. The dynamical evolution behavior of the fundamental, SH, and TH stays nearly the same. Figures 5(c) and 5(d) correspond to the situation at $t = \sqrt{3}$. The maximum of THG is still continuous while the oscillation period of THG experiences a significant transition. Figures 5(e) and 5(f) correspond to the situation at $t = 3$; nonetheless, both the maximum and the oscillation period of THG are discontinuous on the boundary θ_B.

III. CONCLUSIONS

In conclusion, we systematically studied the MQPM THG and proposed a full theory. All the 24 cascaded THG configurations are grouped into three categories according to their common coupling characteristics. Except for category I, the other two categories are all polarization dependent. Physical properties such as controllable efficient THG and QPM gap effect are predicted. The theoretical results may be interesting in fundamental physics and hopefully have potential applications in nonlinear photonics.

ACKNOWLEDGMENTS

This work is supported by the State Key Program for Basic Research of China (Grant No. 2010CB630703), the National Natural Science Foundation of China (Grants No. 11074120 and No. 11074118), and the Doctoral Fund of Ministry of Education of China (Grant No. 20090091110043).

[1] D. Shechtman, I. Blench, D. Gratias, and J. W. Cahn, Phys. Rev. Lett. **53**, 1951 (1984).
[2] C. Janot, *Quasicrystals* (Clarendon Press, Oxford, 1992).
[3] P. J. Steinhardt, and S. Ostlund, *The Physics of Quasicrystals* (World Scientific, Singapore, 1997).
[4] C. B. Clausen, Y. S. Kivshar, O. Bang, and P. L. Christiansen, Phys. Rev. Lett. **83**, 4740 (1999).
[5] A. D. Villa, S. Enoch, G. Tayeb, V. Pierro, V. Galdi, and F. Capolino, Phys. Rev. Lett. **94**, 183903 (2005).
[6] M. Bayindir, E. Cubukcu, I. Bulu, and E. Ozbay, Phys. Rev. B **63**, 161104(R) (2001).
[7] S. N. Zhu, Y. Y. Zhu, and N. B. Ming, Science **278**, 843 (1997).
[8] S. Longhi, Opt. Lett. **32**, 1791 (2007).
[9] Y. Q. Qin, Y. Y. Zhu, C. Zhang, and N. B. Ming, J. Opt. Soc. Am. B **20**, 73 (2003).
[10] R. Ivanov, K. Koynov, and S. Saltiel, Opt. Commun. **212**, 397 (2002).
[11] C. Zhang, Y. Q. Qin, and Y. Y. Zhu, Opt. Lett. **33**, 720 (2008).
[12] S. D. Setzler, P. G. Schunemann, M. J. Missey, and D. E. Zelmon, *Advanced Solid State Lasers*, OSA Trends in Optics and Photonics Vol. 26, edited by M. M. Fejer, H. Injeyan, and U. Keller (Optical Society of America, Washington, DC, 1999).
[13] S. C. Buchter, T. Y. Fan, V. Liberman, J. J. Zayhowski, M. Rothschild, E. J. Mason, A. Cassanho, H. P. Jenssen, and J. H. Burnett, Opt. Lett. **26**, 1693 (2001).
[14] L. Gordon, G. L. Woods, R. C. Eckardt, R. R. Route, R. S. Feigelson, M. M. Fejer, and R. L. Byer, Electron. Lett. **29**, 1942 (1993).
[15] G. I. Petrov, O. Albert, N. Minkovski, J. Etchepare, and S. M. Saltiel, J. Opt. Soc. Am. B **19**, 268 (2002).
[16] N. G. R. Broderick, R. T. Bratfalean, T. M. Monro, D. J. Richardson, and C. M. de Sterke, J. Opt. Soc. Am. B **19**, 2263 (2002).
[17] C. Zhang, Y. Y. Zhu, S. X. Yang, Y. Q. Qin, S. N. Zhu, Y. B. Chen, H. Liu, and N. B. Ming, Opt. Lett. **25**, 436 (2000).
[18] D. Zhu, C. Zhang, Y. Q. Qin, X. J. Lv, and Y. Y. Zhu (unpublished).